Supplemental Data

APOL1 Variants Change C-terminal Conformational Dynamics and binding to SNARE protein VAMP8

Sethu M. Madhavan[1], John F. O'Toole[1], Martha Konieczkowski[1], Laura Barisoni[2], David B. Thomas[2], Santhi Ganesan[3], Leslie A. Bruggeman[1], Matthias Buck[4], and John R. Sedor[1,4]

[1]Department of Medicine and the Rammelkamp Center for Education and Research, MetroHealth System Campus; [2]Department of Pathology, University of Miami, Miami, FL, USA, [3]Department of Pathology, MetroHealth System Campus; [4]Department of Physiology and Biophysics, Case Western Reserve University School of Medicine, Cleveland, OH, USA.

Supplementary Methods

Plasmid cloning

cDNA clone containing *APOL1* (NM_003661) ORF was purchased from GeneCopoeia (Rockville, MD). PCR mutagenesis was carried out using the Quickchange site-directed mutagenesis kit (Agilent Technologies, CA) to generate *G1* and *G2* plasmids which were subcloned in to vectors to generate various *APOL1* constructs. pEGFP-N2 (Clontech) and pmCherry-N1 (Clontech) plasmids were used to generate C-terminal *GFP*- or *mCherry*-tagged *APOL1* expression vectors: pEGFP-N2-*APOL1*-(*G0*)(1-398), pEGFP-N2-*APOL1*-(*G1*)(1-398), pEGFP-N2-*APOL1*-(*G2*)(1-398), pEGFP-N2-*APOL1*(1-338), pmCherry-N1-*APOL1*-(*G0*)(1-398), pmCherry-N1-*APOL1*-(*G1*)(1-398), pmCherry-N1-*APOL1*-(*G2*)(1-398). GST fusion proteins were generated from the following pGEX4T1 expression plasmids: pGEX4T1-*APOL1*-(*G0*) (305-398), pGEX4T1-*APOL1*-(*G1*) (305-398) and pGEX4T1-*APOL1*-(*G2*) (305-398). C-terminal 6X-His tagged APOL1 (305-398) was generated by cloning *APOL1-G0, -G1* and *-G2* into pET-22b vector (Novagen). pStaby1.2-*APOL1*-(*G0*)-V5-His_6 (28-398) was a gift from Dr. Etienne Pays (Université Libre de Bruxelles, Brussels, Belgium) (1). PCR mutagenesis was carried out as described above to obtain pStaby1.2-*APOL1* vector with *G1* and *G2* mutations. Human *VAMP8-myc-FLAG* and *VAMP1-myc-FLAG* was purchased from Origene (Rockville, MD) and subcloned into pET-28b vector (Novagen) to generate N-terminal 6X-His tagged pET28b-*VAMP8* (1-100) and pET28b-*VAMP8* (1-76) constructs. pET28b-*NHE1* was a gift from Dr. Jeffery Schelling (MetroHealth System, Case Western Reserve University, Cleveland, OH).

Immunohistochemistry, immunofluorescence and immunocytochemistry

Immunohistology was done as previously described (2). Briefly, human kidney tissue fixed in neutral buffered formalin or 4% paraformaldehyde at room temperature overnight was embedded in paraffin using standard protocols. Five micrometer sections on slides were incubated overnight at 42^0C, subsequently deparaffinized and hydrated in a graded ethanol

series and finally incubated in a pressure boiler containing boiling heat-induced epitope retrieval (HIER) buffer (10 mM sodium citrate and 0.05 % tween-20) for 4 minutes. Slides were gradually cooled to room temperature over the next 1-2 hours, washed in phosphate buffered saline (PBS) with 0.2% Tween 20 and blocked in 5% normal serum in PBS-Tween 20 for one hour at room temperature. For immunofluorescence, primary antibody incubation was done overnight in 1% normal serum in PBS followed by appropriate secondary antibodies at room temperature for one hour. Nuclei were stained with TOTO-3-iodide (Invitrogen). For immunoperoxidase staining, after antigen retrieval, endogenous peroxidase activity was quenched with 3% hydrogen peroxide followed by blocking and incubation with primary antibody overnight. Vectastain ABC kit (Vector laboratories, Burlingame, CA) was used according to manufacturer's instructions for secondary antibody staining followed by color development with 3, 3'-diaminiobenzidine (DAB) horseradish peroxidase (HRP) substrate. For immunocytochemistry, cells on coverslips were fixed with 4% paraformaldehyde at 4^0C for 15 minutes followed by permeabilization with 0.2% Triton X-100. Incubation with primary antibodies were carried out at 4^0C overnight followed by appropriate secondary antibodies for one hour at room temperature. Immunofluorescence images were captured using a Leica TCS SP2 confocal system (Leica Microsystems, Wetzlar, Germany) Sections processed for immunohistochemistry were analyzed with Nikon Eclipse E600 microscope (Nikon Instruments Inc.) and images captured with SPOT RT3 camera using SPOT v5.1 software (SPOT Imaging Solutions, Sterling Heights, MI).

Quantification of immunofluorescence imaging

Since APOL1 expression in individual podocytes does not overlap with traditional podocyte markers on a pixel for pixel basis, a semiquantitative estimate of APOL1 co-expression with podocyte markers in individual cells was used. Briefly, confocal images (512 x 512 pixels) of APOL1 and GLEPP1 staining in glomeruli are processed using ImageJ background subtraction

and colocalization finder plugins. The merged image preserved APOL1 and GLEPP1 signal in separate channels; overlapping pixels appear as white. A grid with 256 cells, each measuring 32 x 32 pixels, was layered over the merged image and the contents of each square were scored as red (GLEPP1) alone, green (APOL1) alone, white representing red and green together. Using a single grid square as a boundary, this analysis permitted an unbiased evaluation of the red and green fluorescence signal proximity and provided a surrogate measure for co-expression in the same cell. Grid squares containing a single fluorescence signal were scored as no colocalization between podocyte markers and APOL1. Cells containing white pixels or both red and green pixels represent co-expression in the same cell. The number of grid squares, in which signal from both channels are present, was divided by the total number of grid squares that touch a glomerulus, and the result is reported in percent as a proximity frequency score. All glomeruli were counted in each biopsy section. Proximity frequency scores from each biopsy within a disease category are presented as means +/- SEMs.

In situ hybridization

In situ hybridization was done on serial sections from normal human kidney tissue obtained during tumor nephrectomies. Tissue samples were immediately processed and ischemia time was limited to less than 30 minutes. Kidney tissue was cut into approximately 0.5 cm x 0.5 cm samples and fixed in 4% methanol free paraformaldehyde (Electron Microscopy Sciences, Hatfield, PA) for 4 hours at 4^0C. Tissue was washed in PBS, dehydrated in ethanol gradients, cleared with xylene and paraffin-embedded. Five micrometer sections were incubated at 42^0C overnight and stored at -70^0C.

APOL1 sense and antisense cRNA probes were generated as previously described (3-5). *APOL1* (nt185-1279 from NM_003661) was amplified using PCR primers with *EcoRI* and *BamHI* overhangs and cDNAs were subsequently cloned in the same orientation into pSPT18 and pSPT19 vectors (Roche Life Sciences, Indianapolis, IN), linearized using restriction

enzymes *EcoRI* and *BamHI*. The correct orientation of inserts was confirmed by sequencing. Both vectors were linearized using *BamHI* and digoxigenin-labeled riboprobes were synthesized using the DIG RNA labeling kit (Roche Life Sciences) according to manufacturer's instructions. *APOL1* antisense riboprobes were synthesized using T7 RNA polymerase from linearized pSPT18 and *APOL1* sense riboprobes were synthesized with SP6 RNA polymerase from linearized pSPT19. Probes were quantified and aliquots were stored at -70^{0}C to avoid freeze/thaw cycles.

The following buffers were used as described below; (1) 20X SSC-3M sodium chloride, 0.3 M sodium citrate; (2) prehybridization buffer- 4X SSC, 45% formamide, 0.01% herring sperm DNA, 0.01% tRNA; (3) hybridization buffer-4X SSC, 45% formamide, 10% dextran sulfate, 0.01% herring sperm DNA, 0.01% tRNA; (4) RNAse buffer-10 mM Tris, 1 mM EDTA, 500 mM NaCl, pH 8.0; (5) buffer-1: 100 mM Tris, 150 mM NaCl, pH=9.5; (6) buffer-2: 100 mM Tris, 150 mM NaCl, 10 mM $MgCl_2$ pH=9.5. For labeling, slides were deparaffinized in xylene for 30 minutes followed by dehydration in ethanol gradients (100, 95, 75, 50 and 25%), each for 3 minutes. Slides were washed in diethylpyrocarbonate (DEPC)-treated water, post-fixed in 4% methanol-free paraformaldehyde (PFA) and permeabilized by incubating in 4 µg/ml proteinase K (Roche Life Sciences) in 100 mM Tris-HCl, 50 mM EDTA (pH=8) at 37^{0}C for 30 minutes. Slides were washed with PBS and refixed in 4% PFA. For acetylation, slides were incubated in 0.1 M triethanolamine (pH=8) for 5 minutes followed by 0.25% acetic anhydride in 0.1 M triethanolamine for 10 minutes (pH=8). Slides were washed in DEPC-treated water and dehydrated in ethanol gradients and dried. Slides were incubated with prehybridization buffer at 42^{0}C for 2 hours followed by riboprobes at a concentration of 1 µg/ml in hybridization buffer for 16 hours in humidified chamber at 42^{0}C. Slides were washed with 2X SSC at room temperature, 42^{0}C and 55^{0}C three times each for 10 minutes. RNAse digestion of non-hybridized probe was done by incubating slides with 20 µg/ml RNAse in RNAse buffer for 30

minutes at 37^0C. Tissue was blocked with 2% normal goat serum and 0.5X Roche blocking solution (Roche Life Sciences) in buffer-1 for one hour at room temperature. Polyclonal sheep, anti-digoxigenin Fab-fragments conjugated to alkaline phosphatase (1:500, Roche Life Sciences) in buffer-1 containing 1% normal sheep serum and 1 mM levamisole was incubated with the tissue for 4 hours at room temperature. After extensively washing with buffer-1 followed by buffer-2 containing 1 mM levamisole, color development was carried out with NBT/BCIP reagent. Slides were mounted with glycerol based media and viewed with light microscopy using a Nikon Eclipse E600 microscope (Nikon Instruments Inc.) and images captured with a SPOT RT3 camera using SPOT v5.1 software (SPOT Imaging Solutions, Sterling Heights, MI).

Quantification of immunogold particles

Gold particle quantification and labelling specificity in electron micrographs was determined using previously published methods (6, 7). Gold particles were counted in a total of 29 regions of interest within podocytes from four separate normal human kidney sections, incubated with anti-APOL1 antibody, and 15 regions of interest within podocytes from one normal human kidney sections incubated with rabbit IgG. The area of each region of interest was measured using ImageJ. Results are presented as median of gold particles +/- 95% confidence intervals counted in regions of interest for each experimental group and as the mean number of gold particles/μm^2 in regions of interest for each experimental group.

Recombinant protein expression and purification

Full length APOL1-G0, G1 and G2-V5-His recombinant proteins for pulldown assays were expressed in bacterial cells using the pStaby system (Delphi Genetics, Belgium). Plasmids were electroporated in to SE1 expression competent cells (Delphi Genetics, Belgium), and cells containing expression clones were selected and grown in one liter of LB media supplemented with 1% glucose. Expression of recombinant proteins was induced by addition of 1mM isopropyl

β-D-1-thiogalactopyranoside (IPTG) when OD_{600} reached 0.6 and followed by culture for 3 hours at 37^0C. Cells were harvested by centrifugation at 5000x*g* for 10 minutes, resuspended in lysis buffer containing 50 mM Tris-HCl, 6M guanidine hydrochloride and 100 mM NaCl (pH 8) and sonicated. The sonicate was then centrifuged at 5000x*g* for 10 minutes, and the supernatant was incubated with Talon beads (Clontech) for 30 minutes at room temperature with gentle agitation. Beads were collected by centrifugation and washed with lysis buffer followed by phosphate buffered saline. Beads were equilibrated in IP/pull-down buffer described as below. NHE1-His recombinant protein was expressed using NHE1-His plasmid (gift from Dr. Jeffrey Schelling, MetroHealth System, Case Western Reserve University, Cleveland, OH). The expected M_r of each recombinant protein was confirmed by SDS-PAGE followed by Coomassie staining of the gel.

GST-APOL1 constructs as described above were transformed in to E*. coli* BL21 DE3 cells and were grown in LB medium. Protein expression was induced at OD_{600} = 0.6 with 0.25 mM IPTG and the culture was continued for 18 hrs at 25^0C. Bacterial pellets were collected by centrifugation and resuspended in lysis buffer (50 mM Tris, 150 mM NaCl, 2 mM EDTA, 5 mM DTT, 2 % Triton X-100, pH 8) supplemented with protease inhibitor cocktail (Roche). Cells were disrupted by sonication and then centrifuged at 16,000x*g* for 1 hr. The supernatant was filtered using 0.2 µM filter and incubated with Glutathione Sepharose® beads (GE Healthcare Bio-Sciences) for one hour. The beads were extensively washed with lysis buffer and bound protein was eluted with lysis buffer containing 30 mM reduced glutathione (Sigma Aldrich). Eluted protein was dialyzed using a Slide-A-Lyzer® cassette (Thermo Scientific) against suitable buffers for downstream experiments.

pET22-*APOL1* (*305-398)-G0,-G1* and-*G2* constructs were expressed in *E. coli* BL21 DE3 cells. Cells obtained from overnight primary cultures in LB medium were transferred to terrific broth medium and grown at 37^0C. Protein expression was induced with 1 mM IPTG at OD_{600} = 0.6

followed by incubation at 25^0C for 20 hrs. Cells were harvested by centrifugation and were resuspended in lysis buffer (20 mM HEPES, 20 mM imidazole, 200 mM NaCl, 0.35% SDS, 8M Urea, pH 7.4). Resuspended bacterial cells were lysed with sonication followed by incubation at 4^0C overnight with gentle stirring. This solution was centrifuged at 16000x*g* for one hour to collect the solubilized protein in the supernatant and purified using 2 ml of nickel-nitrilotriacetic acid (Ni-NTA) resin (Qiagen), which was equilibrated with lysis buffer for one hour followed by incubation with supernatant for 30 minutes at room temperature. Protein bound to the Ni^2 column was washed with 40 column volumes (CV) of lysis buffer followed by 40 CV of refolding buffer (20 mM HEPES, 20 mM imidazole, 200 mM NaCl, 15 mM dodecylphosphocholine, pH 7.2). Bound protein was eluted from the column in elution buffer (20 mM HEPES, 500 mM imidazole, 200 mM NaCl, 15 mM dodecylphosphocholine, pH 7.2). Eluted protein was concentrated with Amicon® 3 kDa molecular weight cut-off (MWCO) concentrator (EMD Millipore) and injected to a 10/300 Superdex 75™ size-exclusion chromatography (SEC) column (GE Healthcare BioSciences) equilibrated with SEC buffer (20 mM HEPES, 200 mM NaCl, 15 mM dodecylphosphocholine, pH 6.9). Fractions collected after SEC were dialyzed overnight in a buffer containing 50 mM sodium sulfate and 20 mM potassium phosphate at pH 6.8 and used in circular dichroism (CD) spectroscopy.

Multiple pilot experiments suggested that N-terminal His_6 tag enhances the stability and solubility of VAMP8 during bacterial expression. *E. coli* BL21 DE3 cells transformed with His_6-VAMP8 (1-76) construct was grown in TB medium and protein expression was carried out as above. The bacterial pellet, obtained after growing cells for 18 hrs at 25^0C after induction, was resuspended in lysis buffer [20 mM HEPES, 40 mM imidazole, 500 mM NaCl, 2 mM tris (2-carboxyethyl) phosphine hydrochloride (TCEP) pH 7.2] supplemented with EDTA free protease inhibitor cocktail (Roche). Cells disrupted by sonication were centrifuged at 16000x*g* for 1 hr to collect the supernatant containing the soluble fraction of expressed protein. The supernatant,

after filtering using a 0.2 µm filter, was loaded onto a 2 ml Ni-NTA resin column equilibrated with the lysis buffer and incubated for one hour at 4^0C. Protein bound to the column was washed with lysis buffer (10 CV x 1, 20 minutes) and wash buffer containing 20 mM HEPES, 80 mM imidazole, 500 mM NaCl, 2 mM TCEP pH 7.2 (10 CV x 2, 20 minutes each). Protein was eluted from the column by incubation with 2 CV elution buffer (20 mM HEPES, 500 mM imidazole, 500 mM NaCl, 2 mM TCEP, pH 7.2) and eluted protein was concentrated using Amicon® 3 kDa MWCO concentrator (EMD Millipore) to final volume of 500 µL before injecting in to 10/200 Superdex 75® FPLC column equilibrated with FPLC buffer (20 mM HEPES, 200 mM NaCl, 2 mM TCEP, 2 mM EDTA, 0.02% surfactant P20 pH 7.4). Fraction containing His_6-VAMP8 (1-76) was collected and purity was confirmed using SDS-PAGE followed by Coomassie staining of the gel. Peak 3 (**Figure S13**) from size exclusion chromatography was concentrated for downstream experiments. We noted that at concentrations above 220 µM, VAMP8 had high tendency to precipitate. Details regarding purification and characterization are shown in **Figure S13.**

SRA structural homology search

Amino acid residues 31-79 of trypanosomal SRA protein was used as query in HHsenser (Max-Planck Institute, Germany) to search nonredundant protein sequence database which generates an alignment of relatively close homologs using PSI-BLAST (8-11). The alignment generated was forwarded to HHpred, a server that is based on the pairwise comparison of profile HMMs; this algorithm is a highly sensitive method for homology detection or structure prediction and helps make inferences from more remotely homologous relationships. Partly redundant databases of protein family alignments including PDB, PFAM, SMART, PANTHER and COG/KOG were individually searched through HHpred for possible human orthologies.

Molecular Dynamics Simulations

Initial setup

The three dimensional structure of APOL1-G0-(305-398) was generated using the iterative threading assembly refinement server (I-TASSER) (12, 13). A threading program was used to generate three dimensional models of APOL1 as appropriate templates with high homology were lacking for comparative modeling. Templates used by I-TASSER for modeling APOL1 C-terminal domain are listed in **Table S3**. G1 and G2 mutations were introduced in this structure using PyMol (Version 1.8, Schrödinger LLC). Predicted structures generated with the G1 and G2 C-terminal amino acid sequences were similar. The proteins were solvated in an explicitly represented TIP3P water box extending 12 Å from the protein in each direction, which added 7518, 7517 and 7224 water molecules to G0, G1 and G2 respectively. The final dimensions of the water boxes were 68 x 70 x 55 Å for G0 and G1 and 68 x 68 x 54 Å for G2. A total of 29 sodium ions and 21 chloride ions (for G0 and G1) and 28 sodium and 20 chloride ions (for G2). were added to neutralize the solvated system and achieve a final NaCl concentration of 150 mM. Solvation and ionization of the system was performed using VMD v1.9.1. APOL1-339-398 G0, G1 and G2 was modeled separately using I-TASSER and solvated in a similar TIP3P water box, extending 10 Å from the protein in each direction.

To generate three dimensional models of the APOL1 C-terminal region and VAMP8 SNARE domain complex, the crystal structure of the endosomal SNARE complex (PDB: 1GL2) was used as the template. The endosomal SNARE complex structure, 1GL2 consists of a four alpha-helical bundle formed by SNARE domains of VAMP8 (residues 6-66), syntaxin-7 (residues 169-229), Vti1b (residues 140-200) and syntaxin-8 (residues 149-209). APOL1 C-terminal residues 339-398 and VAMP8 SNARE domain (residues 12-68) were aligned based on heptad prediction of residues by MARCOIL and residues from the template (1GL2) were mutated to APOL1 residues using PyMol. Missing residues in the C-terminal end of all helices were added using Swiss PDB viewer to cover the entire length of the APOL1 C-terminal (339-398). Despite the initial alignment we found that a further adjustment was necessary: the alpha helix formed by

residues 365-398 of APOL1 was rotated by 180 degrees on the parent template to optimize distribution of charged residues in the complex and joined to N-terminal residues of APOL1 using MODLoop. The final model of the complex has APOL1 C-terminus and VAMP8 SNARE domain in parallel orientation and varying stoichiometry (3:1 and 1:3). The VAMP8 helix in the endosomal SNARE complex was preserved in all models while other helices were mutated to APOL1 or VAMP8 based on the intended stoichiometry. All models were solvated in TIP3P water box extending 10 Å from the protein followed by addition of sodium and chloride ions to neutralize the system and to a final concentration of 100 mM. Our efforts to model this complex using early endosomal (PDB ID: 2NPS) and neuronal synaptic fusion SNARE complex (PDB ID: 1SFC) failed due to steric clashes likely originating from closer packing of the four alpha helical bundles in these structures.

Minimization and Equilibration

The system was relaxed by 5000 steps of energy minimization to remove the strain in the initial structure before the MD simulations. Protein atoms were then fixed and the system was equilibrated for 50 ps, followed removal of the constraints and equilibration for 200 ps at 50 K with a time step of 2 fs. The system was heated from 50 K to 300 K over 200 ps and equilibrated for 400 ps.

Production stage

MD simulations were done using CHARMM27 force field with CMAP correction in NAMD v2.9 with a timestep of 2 fs (14, 15). For non-bonded calculations, a cutoff distance of 12 Å was used with a smooth switching function initiated at 10 Å. The standard particle-mesh Ewald method was applied to calculate the long-range electrostatic interactions. All bonds, involving hydrogen, were kept rigid using the SHAKE algorithm. All simulations were carried out under isothermal-isobaric conditions (NPT ensemble) by maintaining temperature at 300K by Langevin dynamics

and constant pressure of 1 atm by employing Nose-Hoover Langevin Piston method. To confirm the results, multiple simulations with random seeds were carried out as in **Table S4**.

Trajectory analysis

Analysis of MD simulation trajectories were done using VMD, Wordom and Carma and plotted using Origin 9.1. Cα-Principal component analysis was done using Wordom, confirmed with Carma and plotted with Origin 9.1. Backbone RMSD values were calculated separately for each simulation. Averaged Cα-RMSF values (from two 20 and two 40 ns MD simulations) were calculated over the last 10 ns of the MD simulations to avoid confounding data resulting from large fluctuations during initial minimizations. De novo polar and hydrophobic contacts formed between helices were identified using PyMol by comparing the starting and final structures and distances between donor and acceptor atoms during simulation were calculated using Wordom. Molecular dynamics simulations and trajectory analyses were run on High Performance Computing (HPC) system at Case Western Reserve University.

REFERENCES

1. Vanwalleghem G, Fontaine F, Lecordier L, Tebabi P, Klewe K, Nolan DP, et al. Coupling of lysosomal and mitochondrial membrane permeabilization in trypanolysis by APOL1. *Nature Commun.* 2015;6:8078.
2. Madhavan SM, O'Toole JF, Konieczkowski M, Ganesan S, Bruggeman LA, and Sedor JR. APOL1 localization in normal kidney and nondiabetic kidney disease. *J Am Soc Nephrol.* 2011;22(11):2119-28.
3. Bruggeman LA, Ross MD, Tanji N, Cara A, Dikman S, Gordon RE, et al. Renal epithelium is a previously unrecognized site of HIV-1 infection. *J Am Soc Nephrol.* 2000;11(11):2079-87.
4. Ross MD, Martinka S, Mukherjee A, Sedor JR, Vinson C, and Bruggeman LA. Math6 expression during kidney development and altered expression in a mouse model of glomerulosclerosis. *Dev Dyn* 2006;235(11):3102-9.
5. Marras D, Bruggeman LA, Gao F, Tanji N, Mansukhani MM, Cara A, et al. Replication and compartmentalization of HIV-1 in kidney epithelium of patients with HIV-associated nephropathy. *Nat Med.* 2002;8(5):522-6.
6. D'Amico F, and Skarmoutsou E. Quantifying immunogold labelling in transmission electron microscopy. *J Microsc.* 2008;230(Pt 1):9-15.
7. Petralia RS, Esteban JA, Wang YX, Partridge JG, Zhao HM, Wenthold RJ, et al. Selective acquisition of AMPA receptors over postnatal development suggests a molecular basis for silent synapses. *Nat Neurosci.* 1999;2(1):31-6.
8. Soding J, Biegert A, and Lupas AN. The HHpred interactive server for protein homology detection and structure prediction. *Nucleic Acids Res.* 2005;33:W244-W8.

9. Soding J. Protein homology detection by HMM-HMM comparison. *Bioinformatics.* 2005;21(7):951-60.
10. Coles M, Djuranovic S, Soding J, Frickey T, Koretke K, Truffault V, et al. AbrB-like transcription factors assume a swapped hairpin fold that is evolutionarily related to double-psi beta barrels. *Structure.* 2005;13(6):919-28.
11. Remmert M, Biegert A, Hauser A, and Soding J. HHblits: lightning-fast iterative protein sequence searching by HMM-HMM alignment. *Nat Methods.* 2012;9(2):173-5.
12. Roy A, Kucukural A, and Zhang Y. I-TASSER: a unified platform for automated protein structure and function prediction. *Nat protoc.* 2010;5(4):725-38.
13. Yang J, Yan R, Roy A, Xu D, Poisson J, and Zhang Y. The I-TASSER Suite: protein structure and function prediction. *Nat Methods.* 2015;12(1):7-8.
14. Phillips JC, Braun R, Wang W, Gumbart J, Tajkhorshid E, Villa E, et al. Scalable molecular dynamics with NAMD. *J Comput Chem.* 2005;26(16):1781-802.
15. Buck M, Bouguet-Bonnet S, Pastor RW, and MacKerell AD, Jr. Importance of the CMAP correction to the CHARMM22 protein force field: dynamics of hen lysozyme. *Biophys J.* 2006;90(4):L36-8.

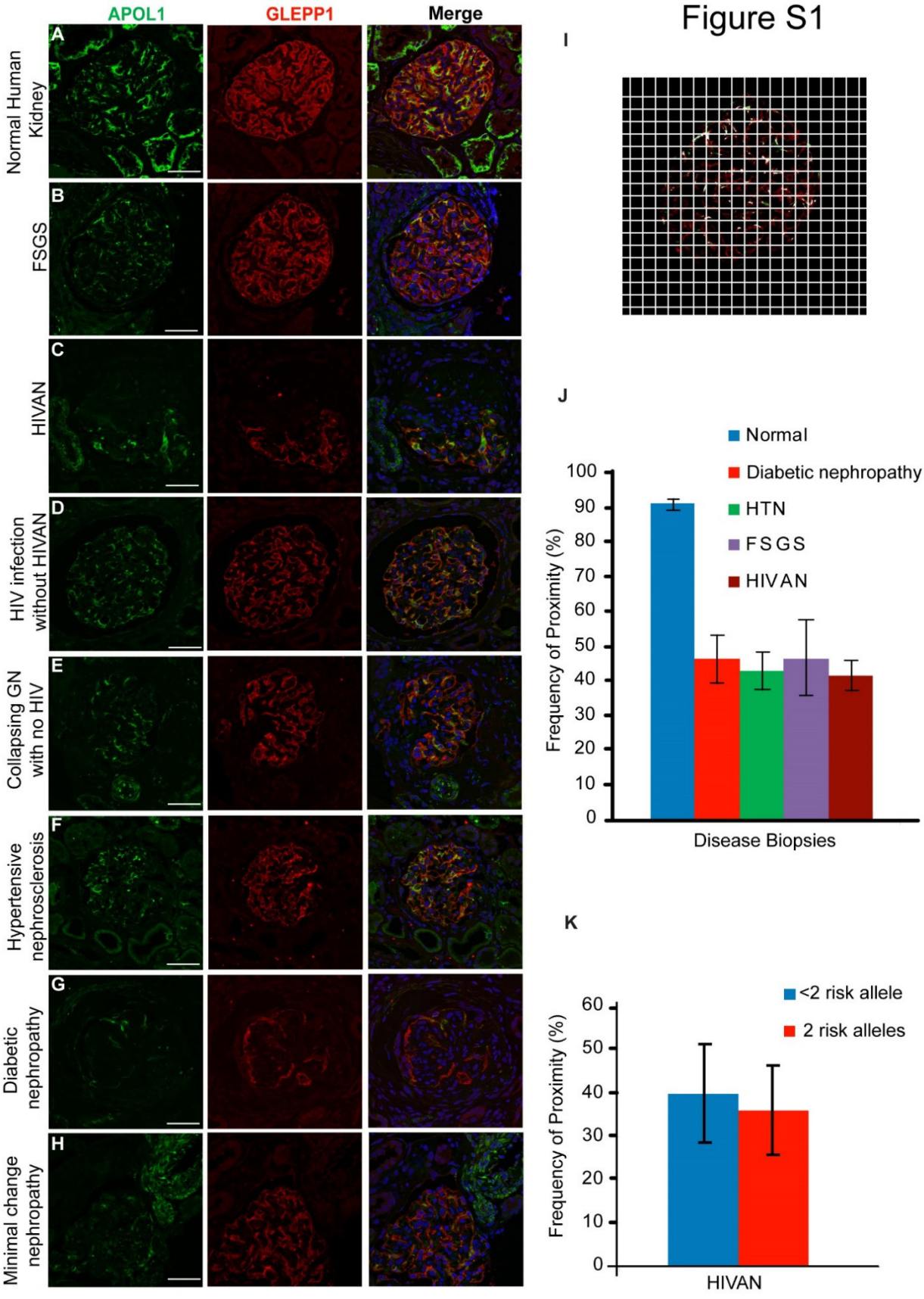
APOL1
GLEPP1
Merge
A
Normal Human Kidney
B
FSGS
C
HIVAN
D
HIV infection without HIVAN
E
Collapsing GN with no HIV
F
Hypertensive nephrosclerosis
G
Diabetic nephropathy
H
Minimal change nephropathy
I
J
Normal
Diabetic nephropathy
HTN
FSGS
HIVAN
Frequency of Proximity (%)
Disease Biopsies
K
<2 risk allele
2 risk alleles
Frequency of Proximity (%)
HIVAN

Figure S1

Figure S1. Glomerular apolipoprotein L1 (APOL1) localization is similar in non-diabetic and diabetic kidney diseases. (A-H) APOL1 (green) and glomerular epithelial protein 1 (GLEPP1) (red) immunofluorescence staining in (A) normal human kidney, (B) focal segmental glomerulosclerosis (FSGS), (C) HIV-associated nephropathy (HIVAN), (D) HIV infection without HIVAN, (E) collapsing glomerulonephritis (GN) without HIV, (F) hypertensive nephrosclerosis, (G) diabetic nephropathy, and (H) minimal change disease. APOL1 staining is diminished in glomerulus in all disease states but remains localized within GLEPP1-labelled podocytes (scale bars: 50 μm). (I) The proximity of glomerular APOL1 and GLEPP1 expression were systematically assessed in images of human kidney glomeruli, both normal and with disease (see Supplemental Methods). Each glomerulus was overlaid with a grid with cell sizes of 32 X 32 pixels. Grid squares, positive for more than one channel, red and green present in separate pixels within the same grid square, or white, representing a pixel positive for both GLEPP1 (red) and APOL1 (green) were counted as preserved proximity, used here as a surrogate measure of positivity in the same podocyte. (J) Bar graph showing mean frequency +/- standard error of APOL1 and GLEPP1 pixel proximity in individual images of glomeruli from normal kidney (n=6), diabetic nephropathy (n=12), hypertension associated chronic kidney disease (n=5), FSGS (n=8), and HIVAN (n=12). APOL1 localized within podocytes as indicated by proximity to GLEPP1 in healthy kidney and proximity was reduced to a comparable degree in all kidney disease states. (K) Pixel proximity for APOL1 and GLEPP1 in HIVAN biopsies was similar between patients with 2 or less than 2 risk alleles. All data are shown as mean ± SEM.

Figure S2

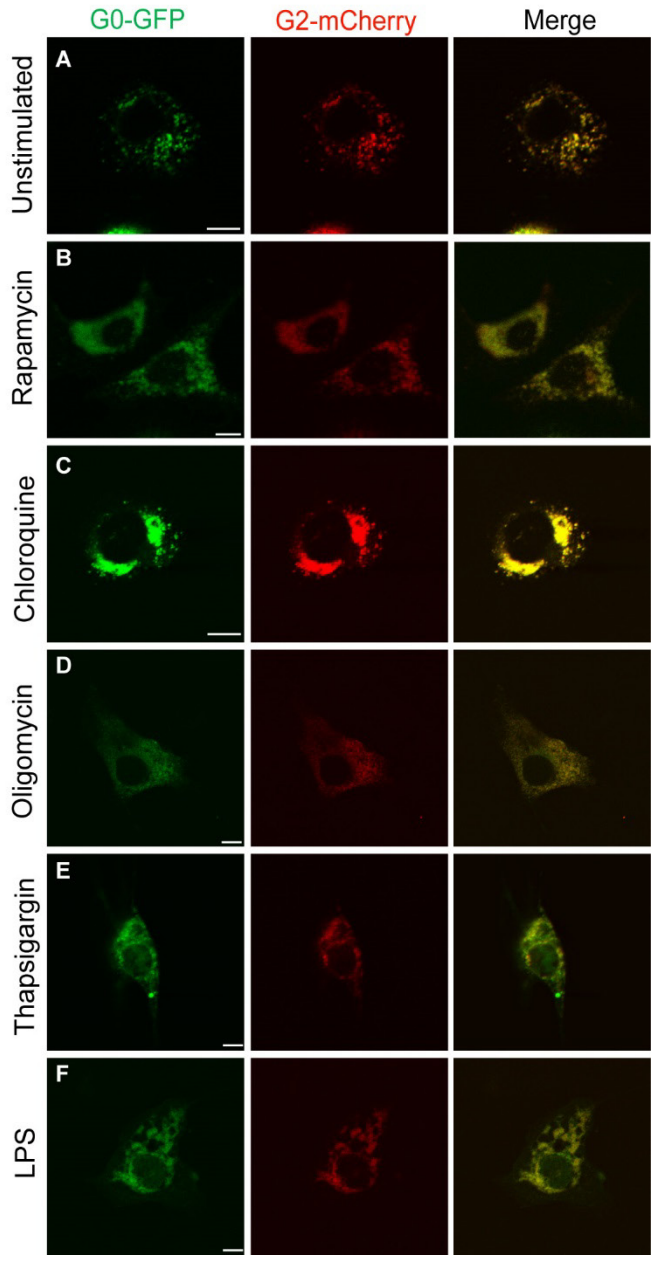

Figure S2. Reference and variant apolipoprotein L1 (APOL1) remain colocalized in the presence of chemically induced cell stress. (A-F) GFP-tagged APOL1-G0 and mCherry-tagged APOL1-G2 proteins were co-localized under basal conditions (A) and after treatments to induce cell stress with rapamycin (B), chloroquine (C), oligomycin (D), thapsigargin (E), or lipopolysaccharide (LPS) (F) (scale bars: 10 μm).

Figure S3

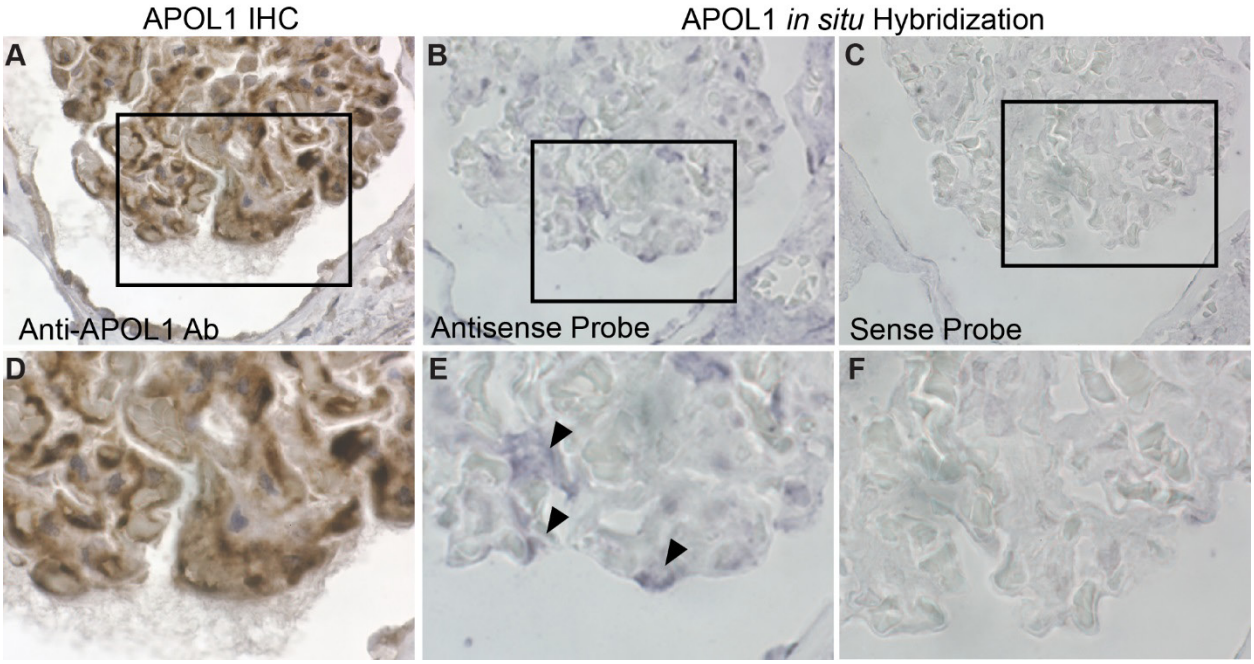

Figure S3. In situ hybridization detecting apolipoprotein L1 (APOL1) mRNA in normal human kidney. (A and D) APOL1 immunohistochemistry (IHC) and (B-C and E-F) in situ hybridization of serial sections from normal human kidney. Immunoperoxidase staining detects APOL1 protein in podocytes (A and D). APOL1 transcripts are detected in podocytes after incubation with antisense probe (B and E), but not in control sections incubated with sense probe (C and F). (Magnification: 100X) (D-F) Selected area of glomerulus from upper panels showing higher magnification detail of staining patterns (Magnification: 185X).

Figure S4

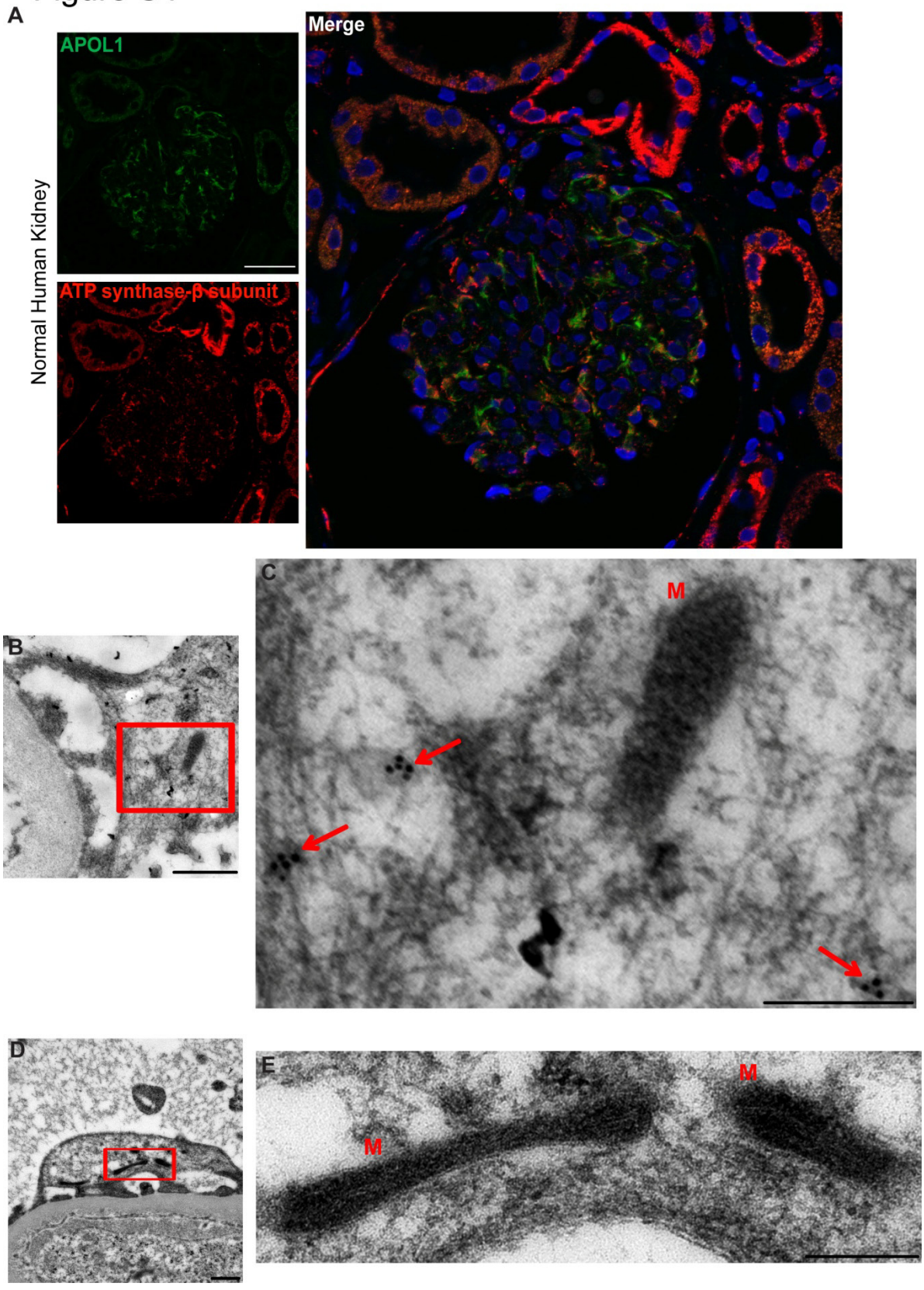
A
Normal Human Kidney
APOL1
ATP synthase-β subunit
Merge
B
C
M
D
E
M
M

Figure S4. Apolipoprotein L1 (APOL1) in normal human kidney detected by immunofluorescent confocal and immunoelectron microscopy. (A) Co-localization of APOL1 (green) with β-subunit of ATP synthase (red), a mitochondrial marker, is seen in proximal tubules but is absent in podocytes. Nuclei stained with TOTO-3 iodide (scale bars: 50 μm). (B-E) Selected region of podocytes in panel B and D showing gold particles in cytoplasm associated with podocyte cytoskeleton indicated by red arrows in (C). No gold particles are detected in the mitochondria denoted by M. (scale bars: (B & D) 0.5 μm and (C & E) 0.2 μm).

Figure S5

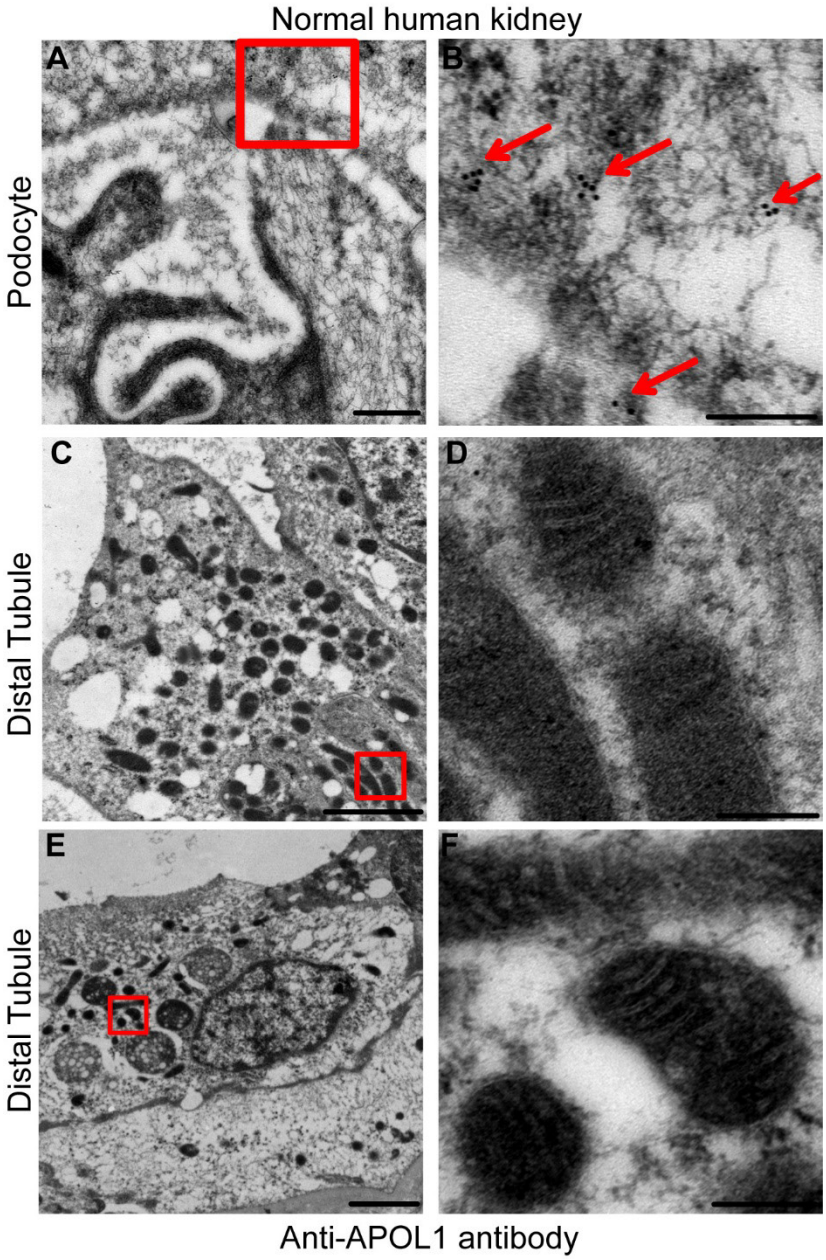

Figure S5. Apolipoprotein L1 (APOL1) in normal human kidney detected by immunoelectron microscopy. (A-B) Selected region of podocytes in panel A showing gold particles in cytoplasm associated with podocyte cytoskeleton denoted by red arrows in (B). (C-F) No gold particles are detected in the distal tubules. Selected area from panel (C) and (E)

shows mitochondria at higher magnification with no gold particles in (D) and (F), respectively. [scale bars: (A,C & E) 2 μm and (B, D & F) 0.2 μm].

Figure S6

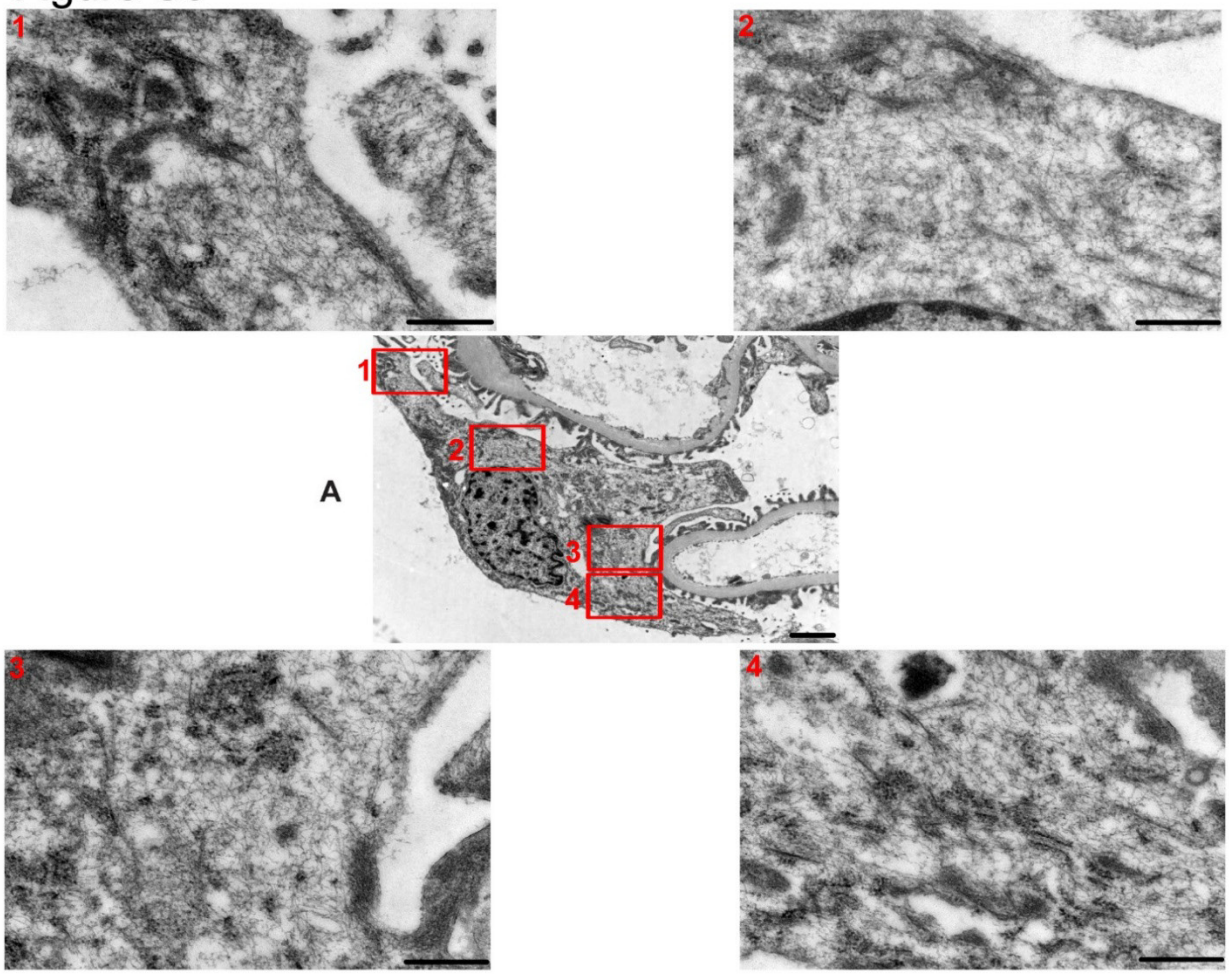
1
2
A
1
2
3
4
3
4

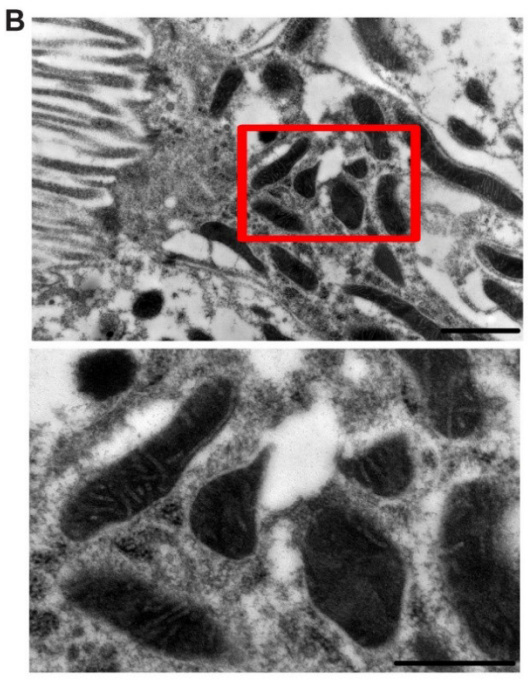
B

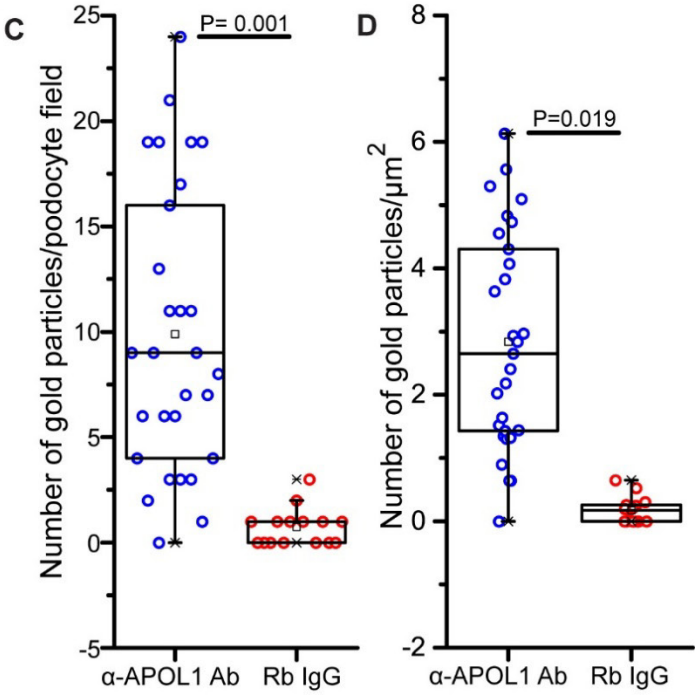
C
P= 0.001
Number of gold particles/podocyte field
25
20
15
10
5
0
-5
α-APOL1 Ab
Rb IgG
D
P=0.019
Number of gold particles/μm2
8
6
4
2
0
-2
α-APOL1 Ab
Rb IgG

Figure S6. Immunoelectron microscopy control and quantification of gold particles/podocyte field and area with anti-apolipoprotein L1 (APOL1) and rabbit IgG. (A-B) Electron micrographs of human kidney sections incubated with rabbit IgG as negative control showing podocyte (A) (scale bar: 2 μm) and proximal tubule (B) (scale bar: 1 μm). High magnification of four selected areas from the podocyte (A) and proximal tubules (B) shows no gold particles (scale bar: 0.5 μm). (C) Box plot showing numbers of total gold particles/podocyte region of interest in normal human tissues incubated with anti-APOL1 antibody (total area = 98.4 μm^2) or rabbit IgG (total area = 71.2 μm^2). (D) Box plot showing number of total gold particles counted per μm^2 in normal human tissues incubated with anti-APOL1 antibody or rabbit IgG. Box plots show quartiles with a median line and 95th percentile whiskers. Wilcoxon rank-sum test was used for statistical analysis.

Figure S7

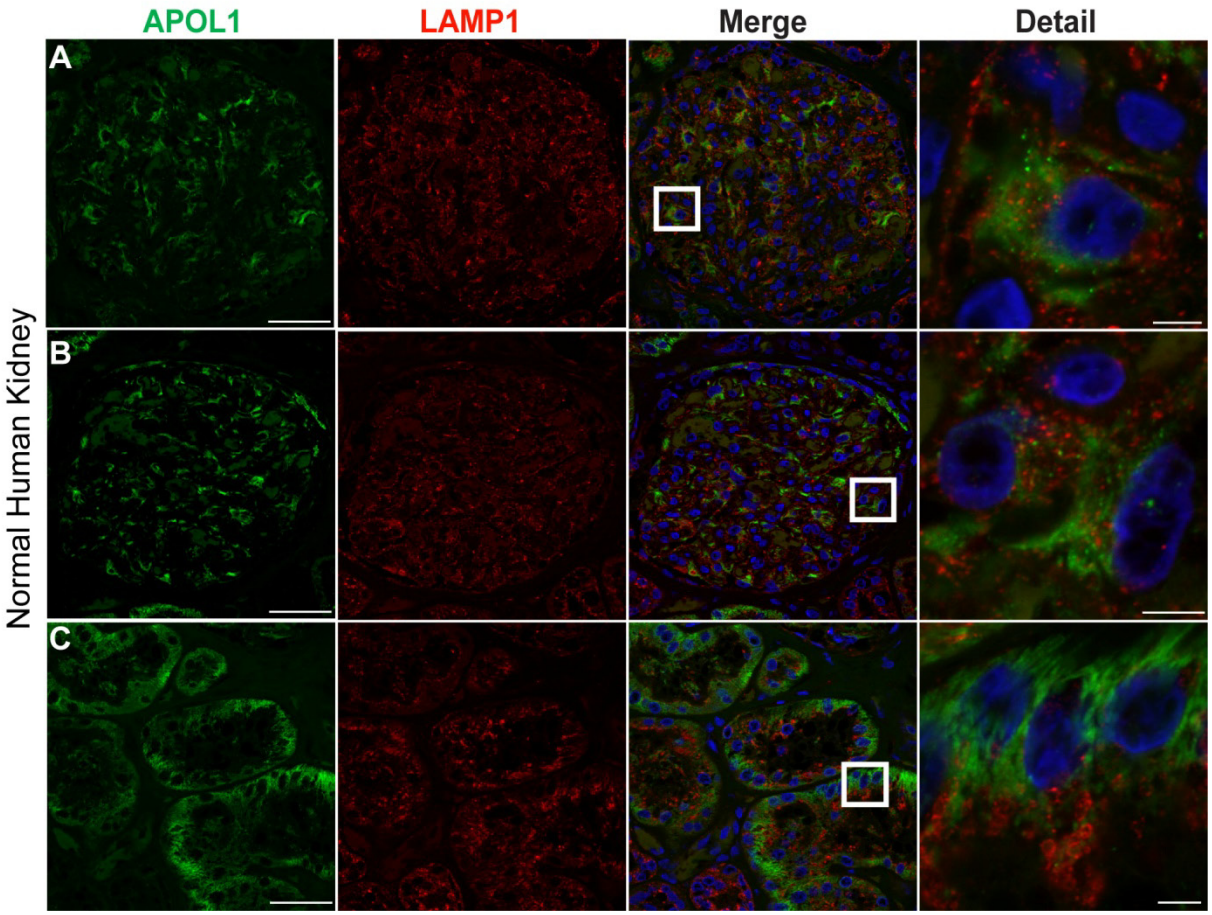

Figure S7. Apolipoprotein L1 (APOL1) does not co-localize with lysosomal marker lysosomal-associated membrane protein 1 (LAMP1) in podocytes. (A-C) Confocal immunofluorescence imaging of normal human kidney sections incubated with anti-APOL1 antibody (green) and anti-LAMP1 antibody (red) shows no colocalization in either podocytes (A-B) or proximal tubules (C) (scale bars: 50 μm). Higher magnification images of the selected regions in glomerulus and proximal tubules are shown in the right most panels (scale bars: 5 μm).

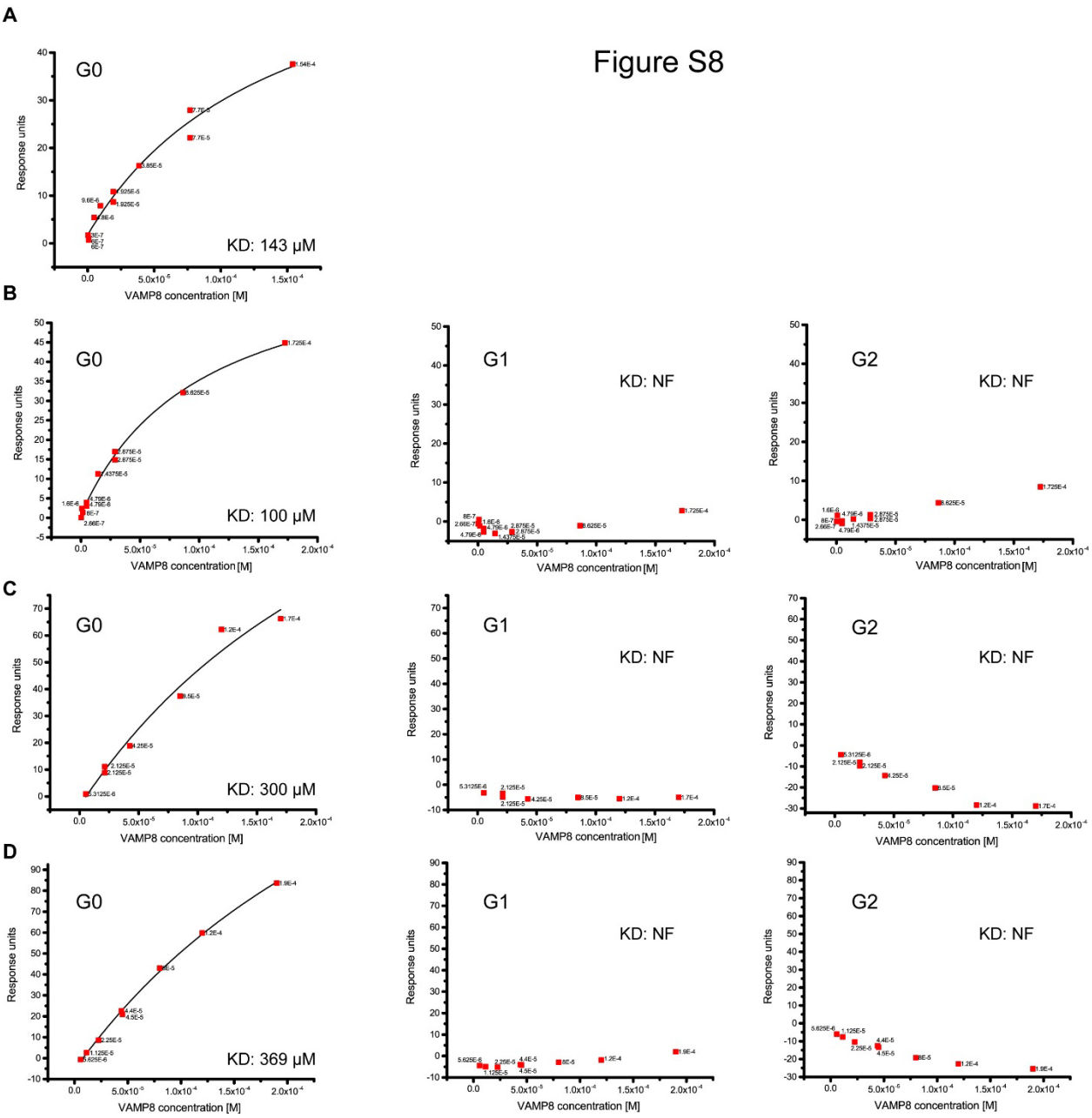

Figure S8

Figure S8. Surface Plasmon resonance (SPR) binding isotherms for amino-terminal GST tagged apolipoprotein L1 (APOL1) (aa 305-398) and amino-terminal 6X-His tagged vesicle-associated membrane protein 8 (VAMP8) (aa 1-76). (A-D) Amino-terminal 6X-His tagged VAMP8 at varying concentrations were injected over the CM5 sensor chip with amino-terminal GST-tagged APOL1 (305-398) G0, G1 or G2 immobilized by amine coupling. Equilibrium response units (Y-axis) were plotted against concentrations of VAMP8 (X-axis).

Dissociation constants (KD) were estimated using steady state affinity analysis by fitting data in to a one-state binding model. (n = 4 for G0 and n = 3 for G1 and G2).

Figure S9

Figure S9. Amino acid sequence of apolipoprotein L1 (APOL1) with domain architecture and location of carboxy-terminal helices. Amino acid sequence of APOL1-G0 (NP_003652.2) showing amino-terminal signal peptide (in italics), pore forming domain (brown) and membrane addressing domain (green). The carboxy-terminal region of APOL1 used for biochemical and biophysical assays and computational modeling is shown in blue. Residues 305 and 339 are marked with arrowheads. Kidney disease associated mutations G1 (S342G & I384M) and G2 (deletion N388 and Y389) are highlighted in red text. The three helices in the carboxy-terminus identified by computational modeling are underlined.

Figure S10

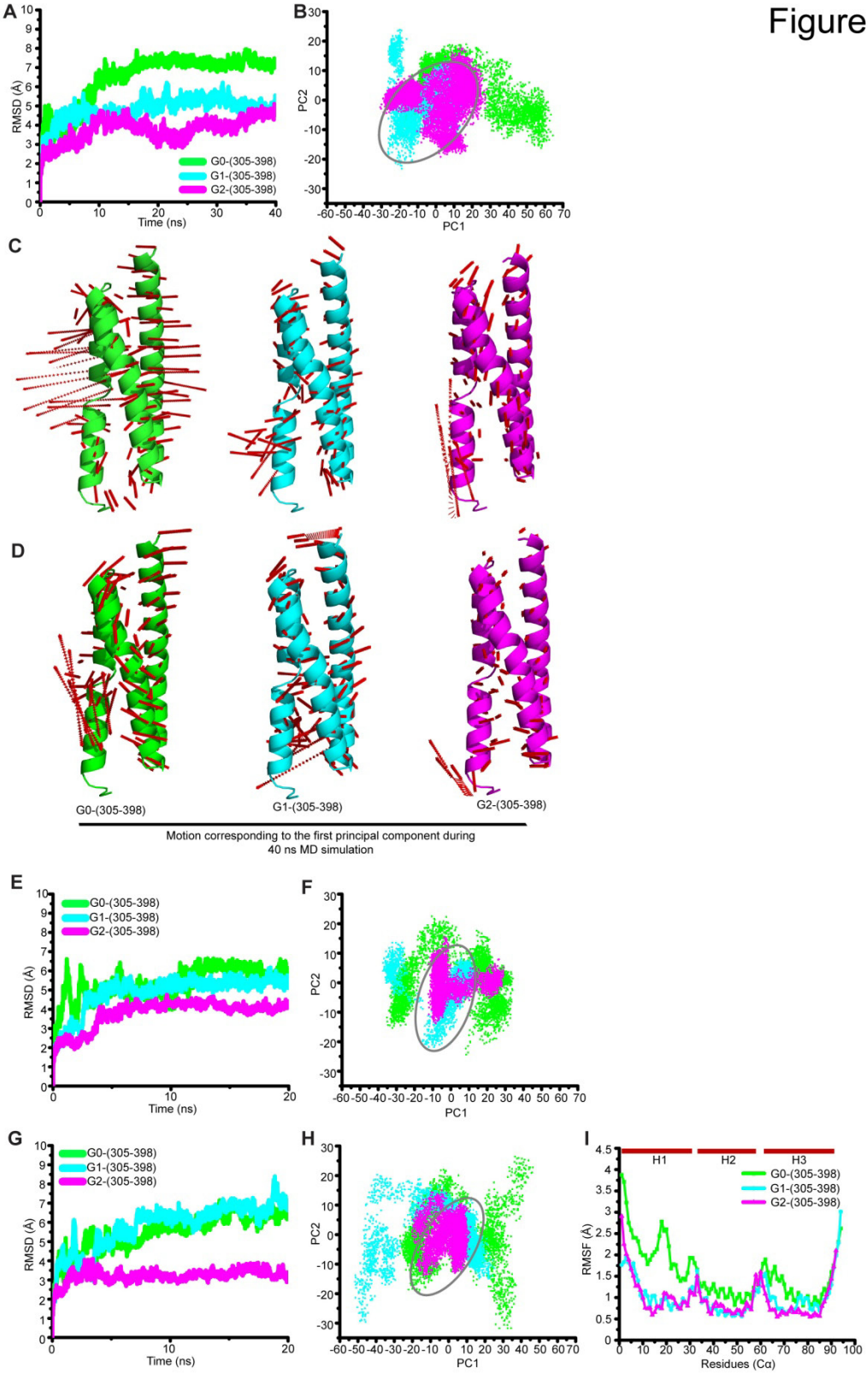
A
RMSD (Å)
Time (ns)
G0-(305-398)
G1-(305-398)
G2-(305-398)
B
PC2
PC1
C
D
G0-(305-398)
G1-(305-398)
G2-(305-398)
Motion corresponding to the first principal component during
40 ns MD simulation
E
RMSD (Å)
Time (ns)
G0-(305-398)
G1-(305-398)
G2-(305-398)
F
PC2
PC1
G
RMSD (Å)
Time (ns)
G0-(305-398)
G1-(305-398)
G2-(305-398)
H
PC2
PC1
I
H1
H2
H3
RMSF (Å)
Residues (Cα)
G0-(305-398)
G1-(305-398)
G2-(305-398)

Figure S10. Trajectory analysis of apolipoprotein L1 (APOL1) -G0, -G1 and -G2 (305-398) obtained from independent 20 ns and 40 ns molecular dynamics (MD) simulations. (A) Conformational changes of APOL1-G0 (green) and APOL1-G1 (blue), and -G2 (red) variants calculated by RMSD values over the 40 ns MD simulations. (B) Projection of the first and second principal components derived from alpha carbon (Cα)-only principal component analysis (PCA) of APOL1-G0, -G1 and -G2 C-terminal domain (305-398) during 40 ns MD simulations. Circled region shows close clustering of conformations achieved by APOL1-G1 and -G2 C-terminus (305-398) during MD simulation. (C-D) Projection of the first eigenvector on the starting model showing higher flexibility of the APOL1-G0 C-terminus compared to the APOL1-G1 and -G2 variants in two separate 40 ns MD simulations. (E-I) Analysis of two 20 ns MD trajectories with random seeds showing higher flexibility of carboxy-terminus (amino acids 305-398) of APOL1-G0 with higher root mean square deviation (RMSD) values (E and G) and Cα PCA projection compared to G2 (F and H). APOL1-G1 showed conformational behavior similar to APOL1-G0 in these simulations; however, flexibility of Cα residues shown by calculating mean root mean square fluctuation (RMSF) values during the last 10 ns (I) of the two separate 20 ns MD simulation is higher for APOL1-G0 residues predominantly belonging to helix 1 (H1) and helix 3 (H3) compared to the APOL1-G1 and -G2 variants.

Figure S11

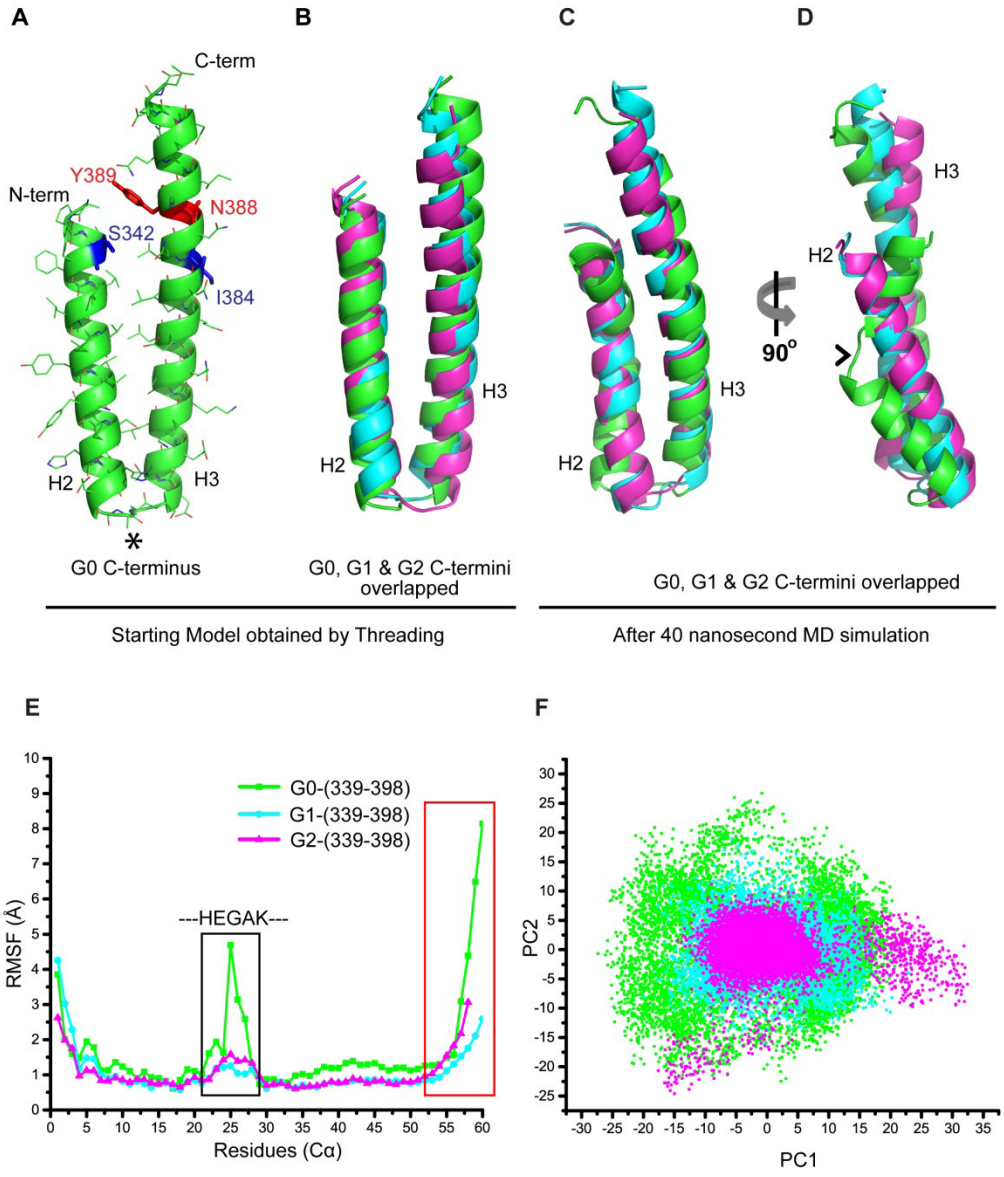

Figure S11. Molecular dynamics (MD) simulation of truncated carboxy-terminus (aa 339-398) of apolipoprotein L1 (APOL1) showing a rigid helical conformation of G1 and G2. (A) Predicted initial structure of APOL1-G0 C-terminal (residues 339-398) obtained by threading shows two α-helices [helix 2 (H2) and helix 3 (H3)] connected by a loop (asterisk). (B) Overlap of initial structures obtained separately by computational modeling shows similar conformation

for APOL1-G0 (green), APOL1-G1 (cyan) and APOL1-G2 (magenta). (C-D) Overlap of final structures of APOL1-G0, APOL1-G1 and APOL1-G2 after a 40 ns MD simulations shows unfolding of the central portion of the APOL1-G0 H2 helix (arrowhead), while the APOL1-G1 and -G2 variant proteins maintain a “closed” conformation. (E) Predominant conformational changes in G0 involve the C-terminal end of H3 (red box) and connecting loop (black box) as shown by the higher root mean square fluctuation (RMSF) of alpha carbon (Cα) atoms of each residue. (F) Projection of MD trajectories (40 ns) of APOL1-G0, -G1 and -G2 C-terminal domain (339-398) on the first and second principal components (PC) derived from Cα-only principal component analysis showing close clustering of the APOL1-G1 and -G2 conformations compared to APOL1-G0.

Figure S12

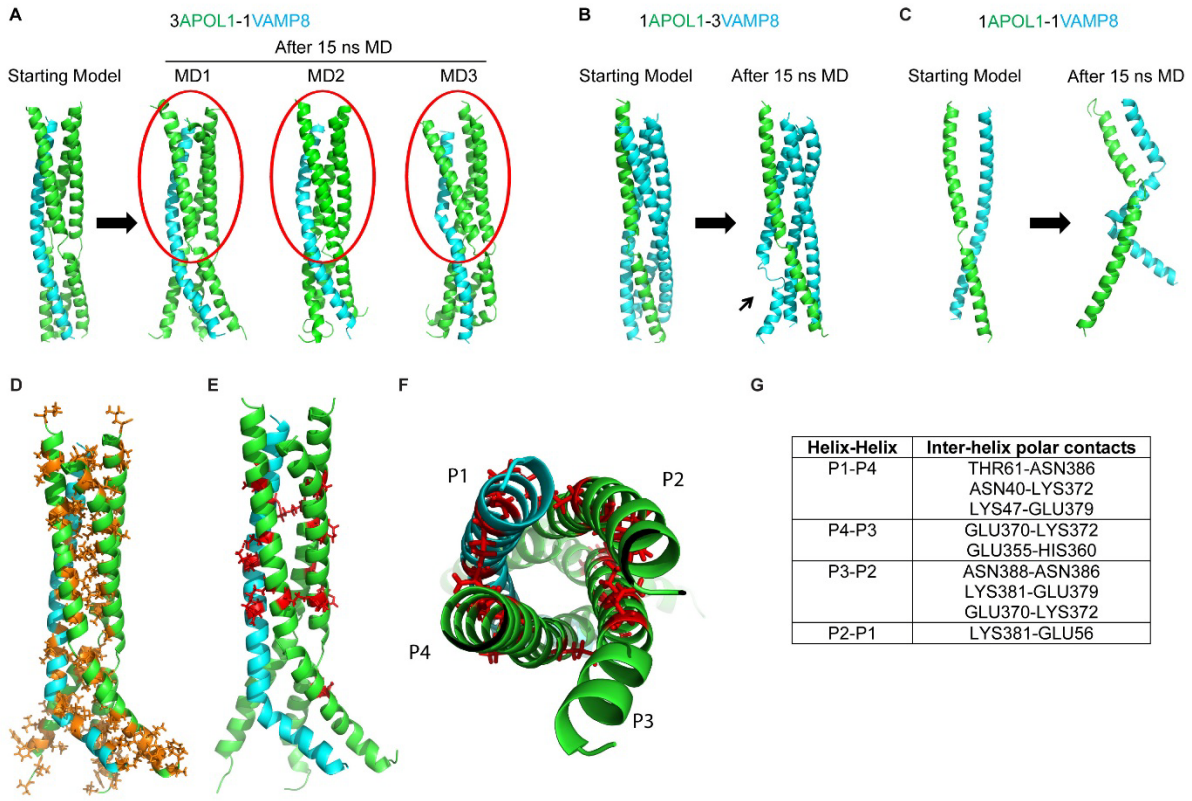

Helix-Helix	Inter-helix polar contacts
P1-P4	THR61-ASN386 ASN40-LYS372 LYS47-GLU379
P4-P3	GLU370-LYS372 GLU355-HIS360
P3-P2	ASN388-ASN386 LYS381-GLU379 GLU370-LYS372
P2-P1	LYS381-GLU56

Figure S12. Molecular dynamics (MD) simulations of APOL1-VAMP8 complex with varying stoichiometry. (A) Starting model of the carboxy-terminus of APOL1-G0:VAMP8 complex was modeled using crystal structure of endosomal SNARE complex (PDB ID: 1GL2) as template. APOL1 is represented in green and VAMP8 in cyan. Helices are in parallel orientation. Final model obtained after a 15 ns MD simulation is shown for APOL1:VAMP8 in a 3:1 stoichiometry (A), a 1:3 stoichiometry (B), and a 1:1 stoichiometry (C). Helix 3 (H3) of APOL1 G0 forms a stable tetrameric structure with VAMP8 in 3:1 conformation (red ovals) in three separate simulations, MD1-MD3 (A). The VAMP8 helix undergoes significant uncoiling (arrow) in the 1:3 APOL1:VAMP8 complex stoichiometry (B), and a major distortion in the 1:1 complex stoichiometry (C). (D) Analysis of the final structure of the 3:1 APOL1:VAMP8 complex shows hydrophobic residues (yellow) packed in the core of the tetramer. (E) Inter-helix polar contacts stabilizing the complex formed by hydrophilic residues (red) that face outwards in the

complex. (F) Top view of (E) showing the *bridge* formed by inter-helix polar contacts (red). (G) List of reproducible inter-helix polar contacts identified from three independent MD simulations of APOL1-G0:VAMP8 complex.

Figure S13

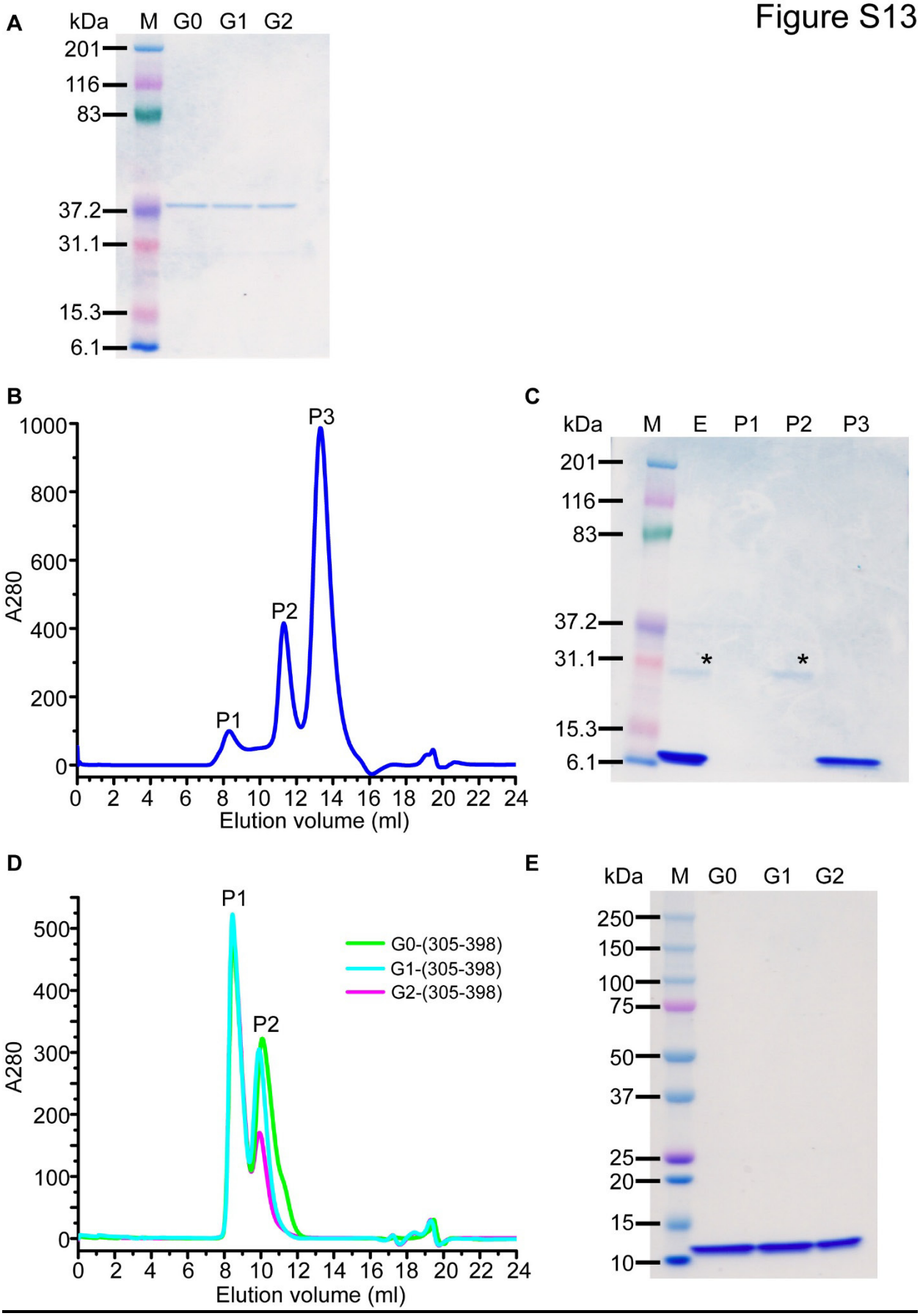
A
kDa
M
G0
G1
G2
201
116
83
37.2
31.1
15.3
6.1
B
A280
Elution volume (ml)
P1
P2
P3
C
kDa
M
E
P1
P2
P3
*
*
D
A280
Elution volume (ml)
P1
P2
G0-(305-398)
G1-(305-398)
G2-(305-398)
E
kDa
M
G0
G1
G2
250
150
100
75
50
37
25
20
15
10

Figure S13. Purification of apolipoprotein L1 (APOL1)-G0, G1 and G2 and vesicle associated membrane protein 8 (VAMP8). (A). Coomassie stained SDS-PAGE gel showing purified GST-G0, -G1, -G2) proteins (aa 305-398). (B-C) Purification of 6X-His-tagged VAMP8 (aa 1-76) by size exclusion chromatography (SEC) using Superdex 75 10/300 GL column (B) Peaks P1, P2 and P3 from size exclusion chromatography were collected and resolved by SDS-PAGE followed by Coomassie staining. A higher band around 30 kDa representing an oligomer or impurities in eluate was removed by SEC (denoted by *). Peak 3 was used for downstream experiments. E denotes eluate obtained from nickel-nitrilotriacetic acid resin (Ni-NTA) column. (D) Size exclusion chromatogram showing elution profile of 6X-His- tagged APOL1-G0, -G1, or -G2 (aa 305-398) recombinant proteins purified from bacterial cells on a Superdex 75 10/300 GL column. Peak 2 (P2), which represents an un-aggregated fraction containing G0, G1 or G2, was used for downstream (CD spectroscopy) experiments. (E) SDS-PAGE and Coomassie stained gel of P2. (M denotes protein molecular weight marker).

Table S1: Summary of human diseases examined for APOL1 expression patterns

Diseases Examined	Number of Cases
Normal (Normal tissue adjacent to tumor [n=5])	6
Focal segmental glomerulosclerosis (FSGS)	8
HIV associated nephropathy (HIVAN)	12
HIV infection without HIVAN (TIN-ATN [n=2], TIN[n=2],TIN-pyelonephritis [n=1])	5
Collapsing GN with no HIV infection	6
Hypertensive nephrosclerosis	6
Diabetic nephropathy	9
Minimal change disease	5

(Abbreviations: TIN – Tubulointerstitial nephritis, ATN – Acute tubular necrosis)

Table S2: Results of structural homology search using APOL1 interacting residues of trypanosomal SRA protein

Protein name	Probability Score
VSG iltat 1.24	94.7
VSG mitat 1.2	94.3
VAMP8	37.2
E2 glycoprotein	32.6
Endobrevin	27.5
YKT6	22.9
Osteocalcin	21.7
VAMP1 iso1	20.7
VAMP1 iso3	18.7
SEC22b	18.4

Table S3: Templates generated by I-TASSER for modeling APOL1 C-terminus (aa 305-398)

PDB ID	Protein name	Template residues	Cov
5j1f	Spectrin repeats of plakin domain of plectin	86-190	0.88
5cwc	De novo designed helical repeat protein DHR5	101-198	0.90
5cff	Miranda/staufen Dsrbd5 Complex	3-89	0.91
1dow	Alpha-catenin dimerization domain	14-118	0.93
5hda	Bs69 Coiled Coil-mynd Domain	3-82	0.85
4hwd	Atbag2	1-90	0.93
4egx	Kif1a axonal vesicular transporter	1-38	0.39
3dyj & 4f7g	Talin	70-180	1.00

(Cov represents the coverage of the threading alignment and is equal to the number of aligned residues divided by the length of query protein.)

Table S4: Summary of MD simulations preformed on the C-terminal domain of APOL1

Model	Time and number of simulations	
	40 ns	20 ns
G0 305-398	2	2
G1 305-398	2	2
G2 305-398	2	2
G0 339-398	1	Not Done
G1 339-398	1	Not Done
G2 339-398	1	Not Done

Model	Time and number of simulations
	15 ns
3 APOL1(G0):1 VAMP8	3
1 APOL1(G0):3 VAMP8	1
1 APOL1(G0):1 VAMP8	1
3 APOL1(G1):1 VAMP8	1
3 APOL1(G2):1 VAMP8	1

Table S5: Secondary structure composition of the APOL1 C-terminal domain determined by circular dichroism spectroscopy.

APOL1 Variant (amino acids)	α-helix	β-strand	Turns	Disordered
G0 (305-398)	46.6 %	9.2 %	15.6 %	28.6 %
G1 (305-398)	50.2 %	8.2 %	14.4 %	27.2 %
G2 (305-398)	49.1 %	9.2 %	14.5 %	27.3 %

Full unedited image of blots in Figure 3A

Blot 1

Blot with mouse monoclonal anti-GFP antibody

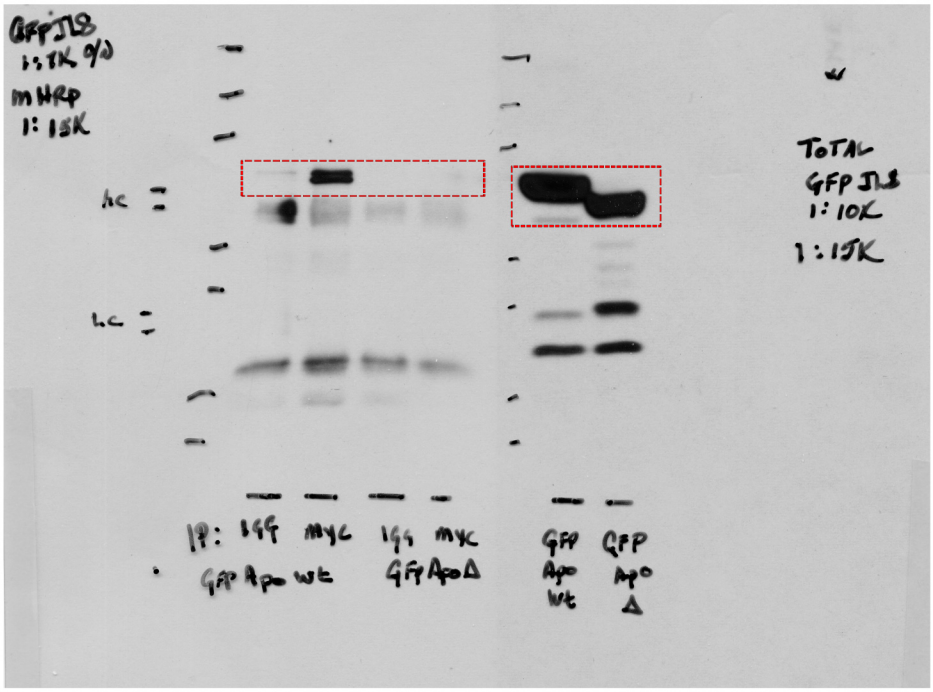

Blot 2

Blot 1 stripped and reprobed with mouse monoclonal anti-FLAG antibody

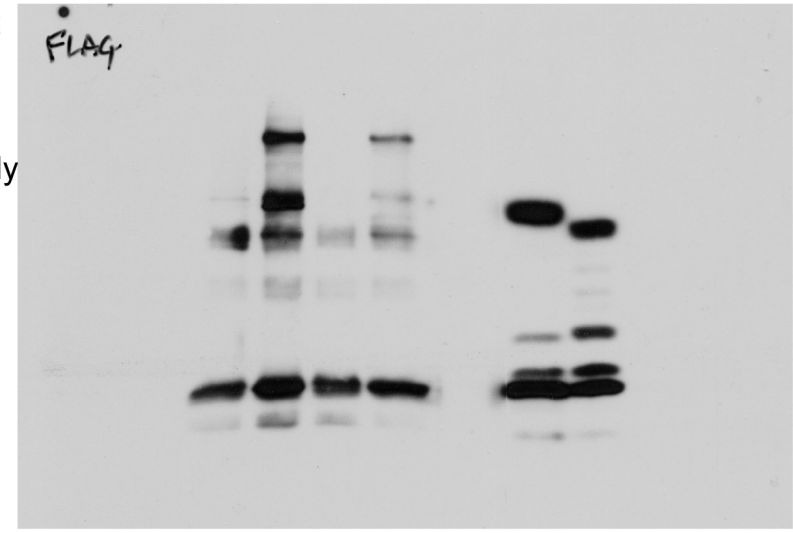

Blot 3

Short exposure of Blot 2

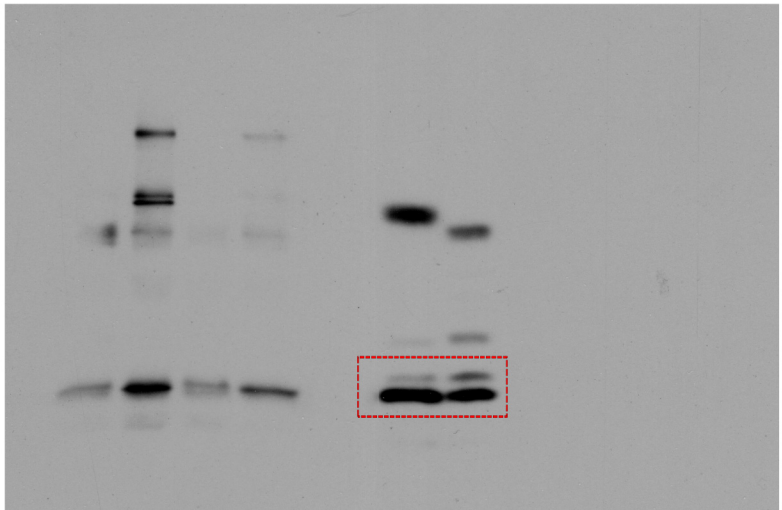

Full unedited image of blots and gel in Figure 4

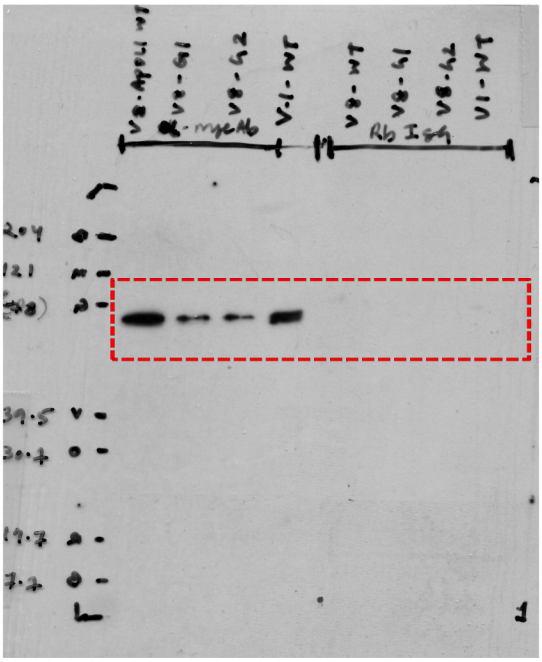

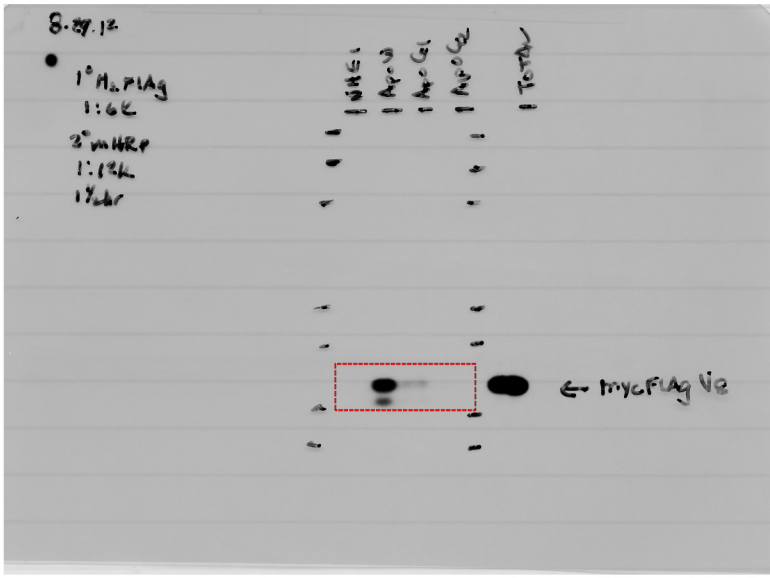

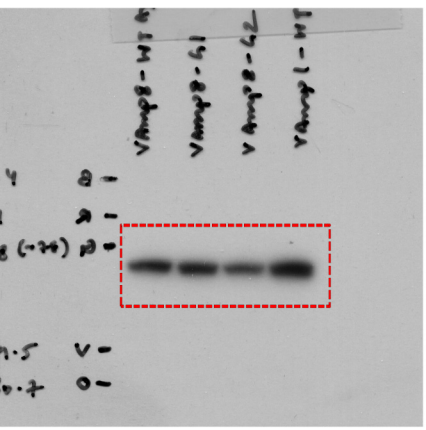

Coomassie stained gel